Remote Sensing of Environment 113 (2009) 306–316

Contents lists available at ScienceDirect

Remote Sensing of Environment

journal homepage: www.elsevier.com/locate/rse

The Al Hoceima (Morocco) earthquake of 24 February 2004, analysis and interpretation of data from ENVISAT ASAR and SPOT5 validated by ground-based observations

A. Tahayt [a,b], K.L. Feigl [b,*], T. Mourabit [a,1], A. Rigo [b], R. Reilinger [c], S. McClusky [c], A. Fadil [d], E. Berthier [e], L. Dorbath [f], M. Serroukh [a], F. Gomez [g], D. Ben Sari [d]

[a] Department of Geology, Faculty of Sciences, Abdelmalek Essaâdi University, M'hannech II, B.P. 2121, 93002 Tetouan, Morocco
[b] UMR5562/DTP, Observatoire Midi-Pyrénées, 14, avenue E. Belin, 31400 Toulouse, France
[c] Department of Earth, Atmospheric, and Planetary Sciences, Massachusetts Institute of Technology, Cambridge, MA 02142, USA
[d] Department of Civil Engineering, Ecole Mohammadia d'Ingénieurs, B.P. 765, Avenue Ibn Sina, Rabat, Morocco
[e] CNRS/LEGOS, Observatoire Midi-Pyrénées, 14, avenue E. Belin, 31400 Toulouse, France
[f] UMR7516, Institut de Physique du Globe de Strasbourg, 5, rue R. Descartes, 67084 Strasbourg, France
[g] Department of Geological Sciences, University of Missouri, Columbia, Missouri 65211, USA

ARTICLE INFO

Article history:
Received 30 June 2007
Received in revised form 24 September 2008
Accepted 27 September 2008

Keywords:
InSAR
ENVISAT
SPOT
GPS
Fault
Earthquake source parameters
Al Hoceima
Morocco

ABSTRACT

The magnitude M_w=6.3 earthquake in Al Hoceima, Morocco of 24 February, 2004 occurred in the active plate boundary accommodating the oblique convergence between Africa and Eurasia. Three different sets of estimates of its source parameters have already been published. We try to resolve the discrepancies between them by using additional data including two remote sensing satellite systems (ENVISAT and SPOT5). Using a model with a dislocation in an elastic half-space, we constrain the source parameters. The hypothesis of two subevents on distinct faults as inferred from seismological inversions is confirmed here by adopting a cross-fault mechanism. The rupture began on a left-lateral strike-slip fault striking at N10° azimuth with 90 cm of horizontal slip and then transferred to a right-lateral strike-slip fault striking at N312° azimuth with 85 cm of horizontal slip. The first fault is at 500 m depth from the free surface and the second fault is at 3 km depth. This model is consistent with ground-based observations, including GPS, seismology, and mapped surface fissures. The pair of faults activated in 2004 appears to constitute part of a complex seismogenic structure striking NNE–SSW that separates the Rif tectonic blocks.

1. Introduction

The Al Hoceima region is now recognized as the most seismically active part of Morocco, due to its situation in the complicated boundary zone between the Eurasia and Africa plates. Its high level of seismicity makes it one of the most studied active zones in the western Mediterranean. The tectonic control of the seismicity is still an open question.

Al Hoceima is located between two major left-lateral strike-slip faults, the Jebha fault striking N70° and the Nekor fault striking N50° (Fig. 1), along which the Rif nappes were transported toward the WSW with left-lateral strike-slip through the Miocene (Leblanc & Olivier, 1984; Frizon de Lamotte et al., 1991). The paucity of seismicity and the lack of Quaternary deposits around these two major geological faults (Leblanc & Olivier, 1984; Frizon de Lamotte et al., 1991) make it difficult to investigate the paleoseismicity and the recent morphotectonics within these prominent structural features of the Rif.

The seismic activity in the Al Hoceima region is characterized by predominantly strike-slip and normal faulting trending from NE–SW to NW–SE (Hatzfeld et al., 1993; Calvert et al., 1997). Historically, the Al Hoceima area has experienced many disastrous earthquakes. Notable sequences in 1522, 1624, 1791 and 1800–1802 have been reported by El Mrabet (2005). On May 26, 1994 a M_w=5.9 earthquake occurred there with a left-lateral strike-slip buried fault (Calvert et al., 1997; El Alami et al., 1998; Bezzeghoud & Buforn, 1999; Biggs et al., 2006; Akoglu et al., 2006). Surface cracks trending mostly from NNE–SSW to NE–SW and coeval with the 1994 main shock have been observed in the epicentral area (Hahou, 2005).

The February 24, 2004 (M_w=6.3) earthquake was one of the most catastrophic of the last century in this region. Its devastating effects included: 629 fatalities, 966 injuries, 2539 destroyed and damaged

* Corresponding author. Present address: Department of Geology and Geophysics, University of Wisconsin-Madison, 1215 W. Dayton St., Madison, WI 53706-1692 USA.
E-mail address: feigl@wisc.edu (K.L. Feigl).
[1] Present address: Department of Geology, Faculty of Sciences and Techniques, Abdelmalek Essaadi University, B.P. 416, Route de Ziaten, km10, Tangier, Morocco.

0034-4257/$ – see front matter © 2008 Elsevier Inc. All rights reserved.
doi:10.1016/j.rse.2008.09.015

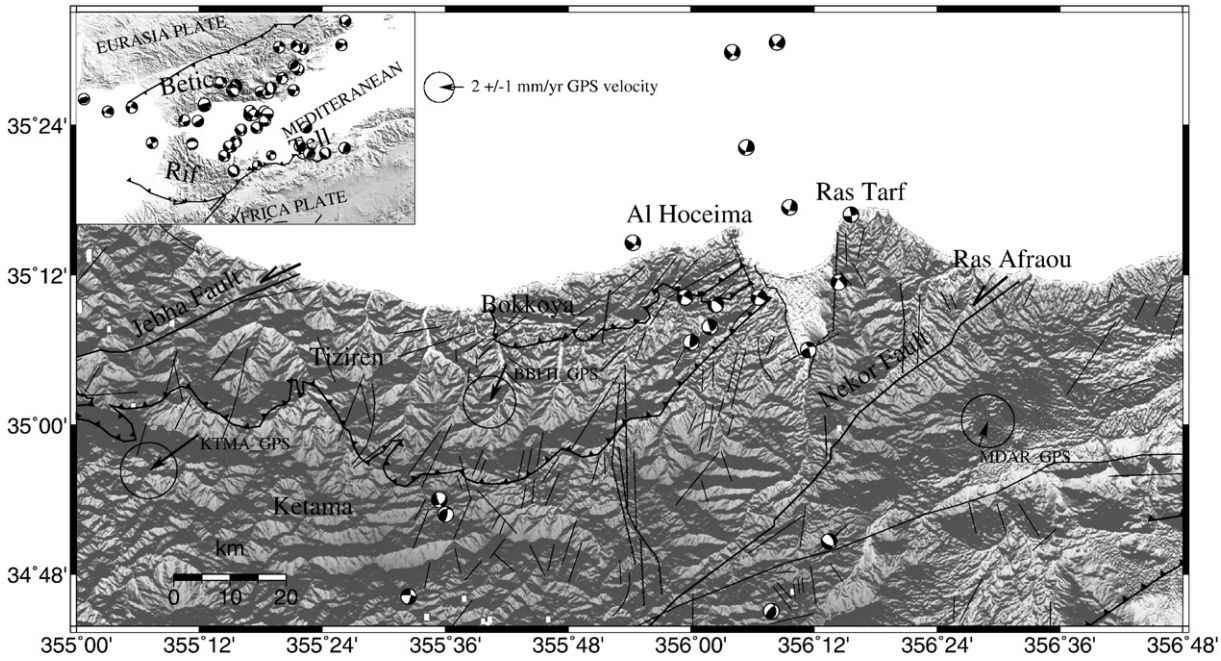

Fig. 1. Tectonic setting of the Al Hoceima (Northern Morocco) region. Focal mechanisms are selected from Stich et al. (2003) and the Harvard (2005) catalog. Tectonic features are from the *Carte des mouvements récents du Rif* (Service Géologique du Maroc, Rabat, 1992). Arrows show velocities of GPS stations for the interval 1999–2005 with respect to Africa plate, with 95% confidence ellipses (Tahayt et al., 2007). The inset shows the regional seismotectonic context of the western Mediterranean Basin. Topography is derived from NASA/SRTM (2005).

houses, and 15,600 homeless. The heavy damage was due in large part to the poor quality of construction combined with site amplification effects. The ground acceleration reached 2.3 m/s/s close to Abdelkarim El Khattabi lake dam located at 20 km SE of Al Hoceima city (CNRST, 2004).

A suite of geophysical studies was undertaken as soon as possible after the Al Hoceima 2004 earthquake using different measurements to determine the source mechanism of the main shock. Jabour et al. (2004) and Aït Brahim et al. (2004) describe the macroseismic effects of the earthquake. Stich et al. (2005) use waveform inversion to estimate the source parameters of the mainshock. They propose a model with two distinct parallel faults striking N11°E. Çakir et al. (2006) estimate the fault geometry and the slip distribution using only descending and ascending synthetic aperture radar (SAR) interferograms to find a curved right-lateral strike-slip fault, striking NW–SE. Biggs et al. (2006) conclude from interferograms and aftershock distribution that the main fault is planar and strikes NW–SE. The differences between these determinations of the source mechanism of the mainshock are due to the complexity of the rupture. Previous solutions for the source parameters are summarized in Table 1.

In this work, we attempt to reconcile these studies by considering most of the available data in a single interpretation. In particular, we analyze data from two satellite systems: ENVISAT and SPOT5. These data constrain an elastic dislocation model to find the source parameters of the earthquake, including the length, width, strike, dip, amount, and rake of the coseismic slip. To validate the interpretation, we compare the model for the earthquake source mechanism to ground-based observations, including seismology, geodesy and geology. Fig. 2 shows the locations of the data sets used in this study.

2. Remotely sensed observations

2.1. InSAR

We use ENVISAT radar images acquired in both descending and ascending tracks before and after the 2004 earthquake to further investigate coseismic deformation (Table 2). Interferometry applied to SAR images (InSAR) yields three coseismic interferograms, two in descending orbital passes and one in an ascending pass. They are

Table 1
Different estimates of source parameters for the 24 February 2004 earthquake in Al Hoceima region using various data sets: (A1) and (A2) are two faults from InSAR, GPS, SPOT5, seismological, and field data (this study); (B) is from InSAR and seismological data (Biggs et al., 2006); (C) is from InSAR data (Çakir et al., 2006); (D1) and (D2) are two faults from seismological data (Stich et al., 2005)

Fault	Longitude (°)	Latitude (°)	Strike (°)	Dip (°)	Rake (°)	Depth* (km)	Length (km)	Width (km)	Slip (m)	Moment ($\times 10^{18}$ N m)	$\bar{R}$
A1 (L)	−3.959	35.122	10	88	1.3	0.5	9	11.5	0.92	2.80	0.0688
A2 (R)	−4.028	35.134	312	88	−179	3.0	15	9.0	0.76	3.08	0.0688
B (R)	−3.986	35.137	295	87	−179	2.1	8.8	16	1.4	6.2	0.0522
C (R)	−3.993	35.127	275–310	88	−161	2	21	16.5	2.7	6.8	0.0302
D1 (L)	−4.000	35.140	11	72	−17	1.6	10	10	1	1.9	
D2 (L)	−4.020	35.140	11	72	−17	0.7	8	8	0.6	1.0	
Z											0.0502

(L) for left and (R) for right, indicate the sense of strike slip.
* Depth of the top edge of the fault. $\bar{R}$ is the mean resultant length of the residual difference between the observed phase and the modeled phase, using a near-field area (Fig. 5). *Z* is the null model.

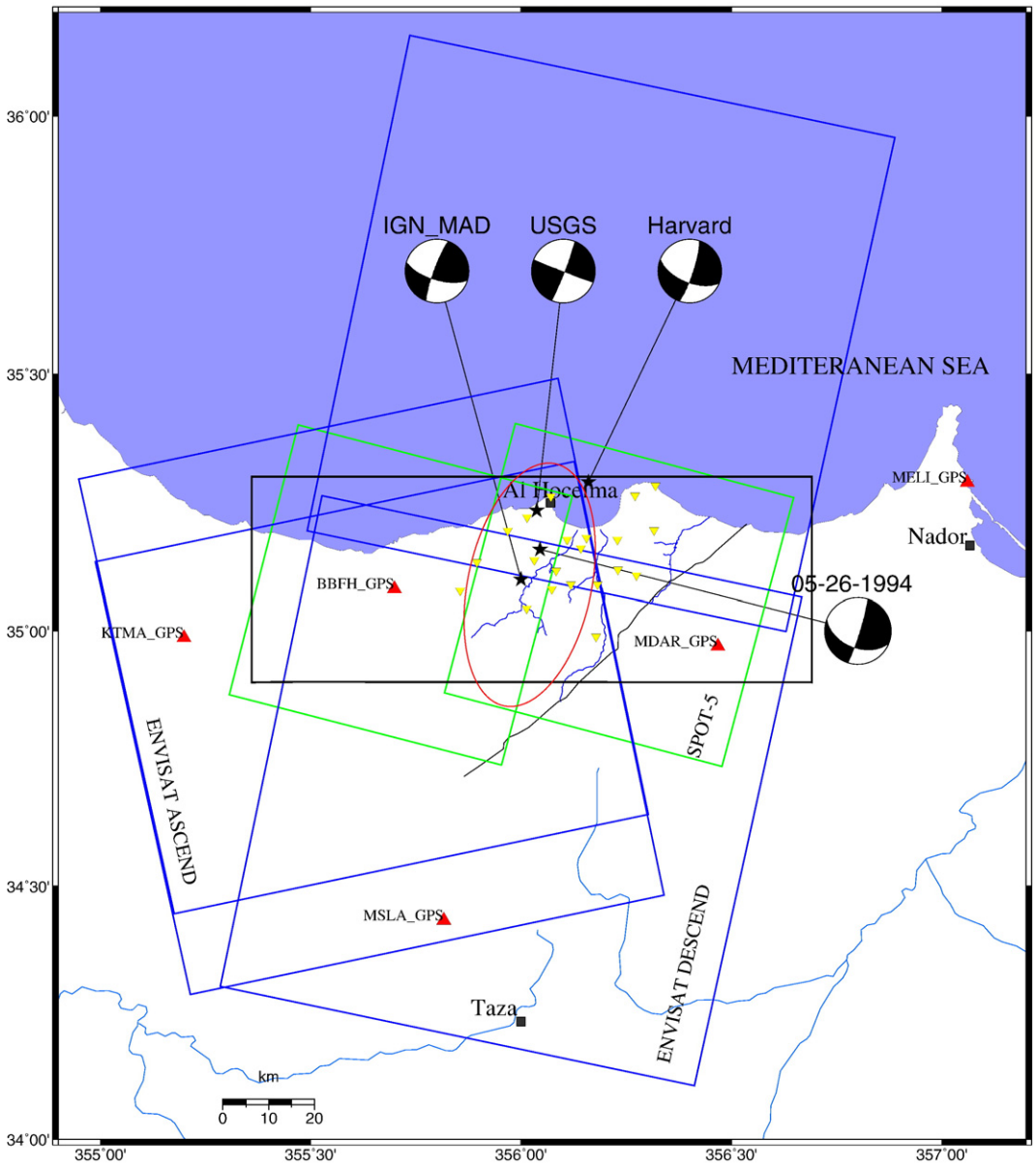

Fig. 2. Data set used in this study. Red ellipse delimits the damaged area. Stars show the epicenter locations of the Al Hoceima main shock (event of February 24, 2004 at 02:27 GMT) with corresponding focal mechanisms estimated by different data centers. Blue rectangles denote subsets of ENVISAT ASAR images in Frames 2889 and 2907 of Track 2880. Green rectangles denote SPOT5 images used in the correlation. Red triangles are GPS stations: MDAR and BBFH have GPS measurements of coseismic displacements included in the modeling. Yellow triangles represent seismic temporary array stations used to collect aftershocks plotted in Fig. 6. Rectangle oriented E–W delimits the area covered by the interferograms shown in Fig. 5.

calculated using the DIAPASON software developed at the French space agency (CNES) using the two-pass method (Massonnet et al., 1993). The interferogram measures the phase change due to differential effects including ground deformation, orbital effects, topographic errors and tropospheric variations that occurred between the two satellite passes. Precise orbits (Scharroo & Visser, 1998) are used to model the orbital effects.

Table 2
ESA ENVISAT data analyzed in this study. Altitude of ambiguity h_a gives the perturbation in topographic elevation required to generate one fringe (Massonnet & Rabaute, 1993)

Pass	Track	Orbit1	Date	Orbit2	Date	h_a (m)	Interval (days)
Ascending	2230	9302	2003-12-10	12308	2004-07-07	518	210
Descending	2280	6847	2003-06-22	12358	2004-07-11	144	385
Descending	2280	5845	2003-04-13	11857	2004-06-06	117	420

We retain two interferograms spanning the date of the 2004 Al Hoceima mainshock (Table 2). These pairs have been presented, along with others, by Biggs et al. (2006) and Çakir et al. (2006) using different methods. The ascending interferogram has a time span of 210 days and an altitude of ambiguity of 518 m. It is the only ascending coseismic pair available in the catalog of ENVISAT images that produces an interferogram with legible fringes. The descending interferogram has a time span of 385 days and an altitude of ambiguity of 144 m. The topographic contribution has been removed using a digital elevation model (DEM) from SRTM3 with an absolute vertical accuracy less than 16 m and a relative vertical accuracy less than 10 m (Falorni et al., 2005). Since these values are a small fraction of the altitudes of ambiguity in the considered pairs, the topographic contribution to the interferometric range change is negligible. Consequently, the topographic contribution from a 10 m 1-σ artefact in the DEM at the epicentral zone would be 0.5 mm or 2 mm for the ascending and descending passes, respectively. The interferometric fringe patterns

record deformation such that each fringe is equal to a change of 28 mm in range along the line of sight between the ground pixel and satellite. The fringes around Al Hoceima region correspond to the coseismic deformation pattern (Fig. 5A). The lobate patterns in the interferograms are compatible with a strike-slip focal mechanism.

Away from the faults, the fringes that appear to "hug" the topography in the mountainous areas south and southwest of the epicenter are probably atmospheric artifacts (e.g., Massonnet & Feigl, 1998). Near the epicenter, the fringes break down into random, decorrelated noise in some of the locations where surface rupture was observed in the field. This phenomenon is especially apparent in the ascending interferogram, where the two NW–SE-trending lobes would converge.

2.1. Measurement of surface strain by correlating optical SPOT5 images

The deformation of the Earth's surface produced by glacier flow, volcanos, landslide movements or earthquakes can be mapped using the correlation of satellite optical images (Van Puymbroeck et al., 2000; Berthier et al., 2005; Binet & Bollinger, 2005; Delacourt et al., 2007). This technique is useful to determine the location and amount of surface rupture on a fault. This technique has been applied to the Izmit 1999 earthquake (Michel & Avouac, 2002) and the Kashmir 2005 earthquake (Avouac et al., 2006). Here, we correlate two images with 2.5-meter resolution from the SPOT5 satellite to investigate the surface deformation produced by the 2004 Al Hoceima earthquake.

The SPOT5 satellite acquired two images of the earthquake area on 18 October 2003 (before the mainshock) and on 16 October 2004 (after the mainshock) in the same orbit. The 364-day time separation is exactly equal to 14 orbital cycles for the SPOT5 spacecraft. This ideal situation (called an "exact repeat pair") leads to a small base-to-height (B/H) ratio of 0.0007, indicating a limited sensitivity to static topographic relief. A typical 10 m error in the SRTM DEM (Falorni et al., 2005) would lead to a distortion of less than 1 cm between the two images after orthorectification. The one-year time separation ensures a similar solar illumination for the two SPOT5 acquisitions, minimizing the errors due to the changes in length of the shadows (Berthier et al., 2005; Delacourt et al., 2007).

To reject any possibility of errors due to the processing strategy, the pair of images were analyzed using two independent software packages: one developed at CNES (Berthier et al., 2005) and Cosi-Corr (Leprince et al., 2007). The main conclusions are similar from both analyses with slightly smaller uncertainties in the results from Cosi-Corr, which are presented here. Windows of 32 by 32 pixels were used to correlate the SPOT5 images with a constant step of 16 pixels in each dimension. Fig. 3 shows the two maps from the correlation analysis, one of the displacement offset in Easting, the second in Northing. The mean shift in both directions is small (about 3 cm) confirming that the two images are co-registered well. No clear offset break appears in either deformation map.

Fig. 4 shows the SPOT estimates of displacement in profiles drawn perpendicular to the strikes of the two candidate faults. The profile most

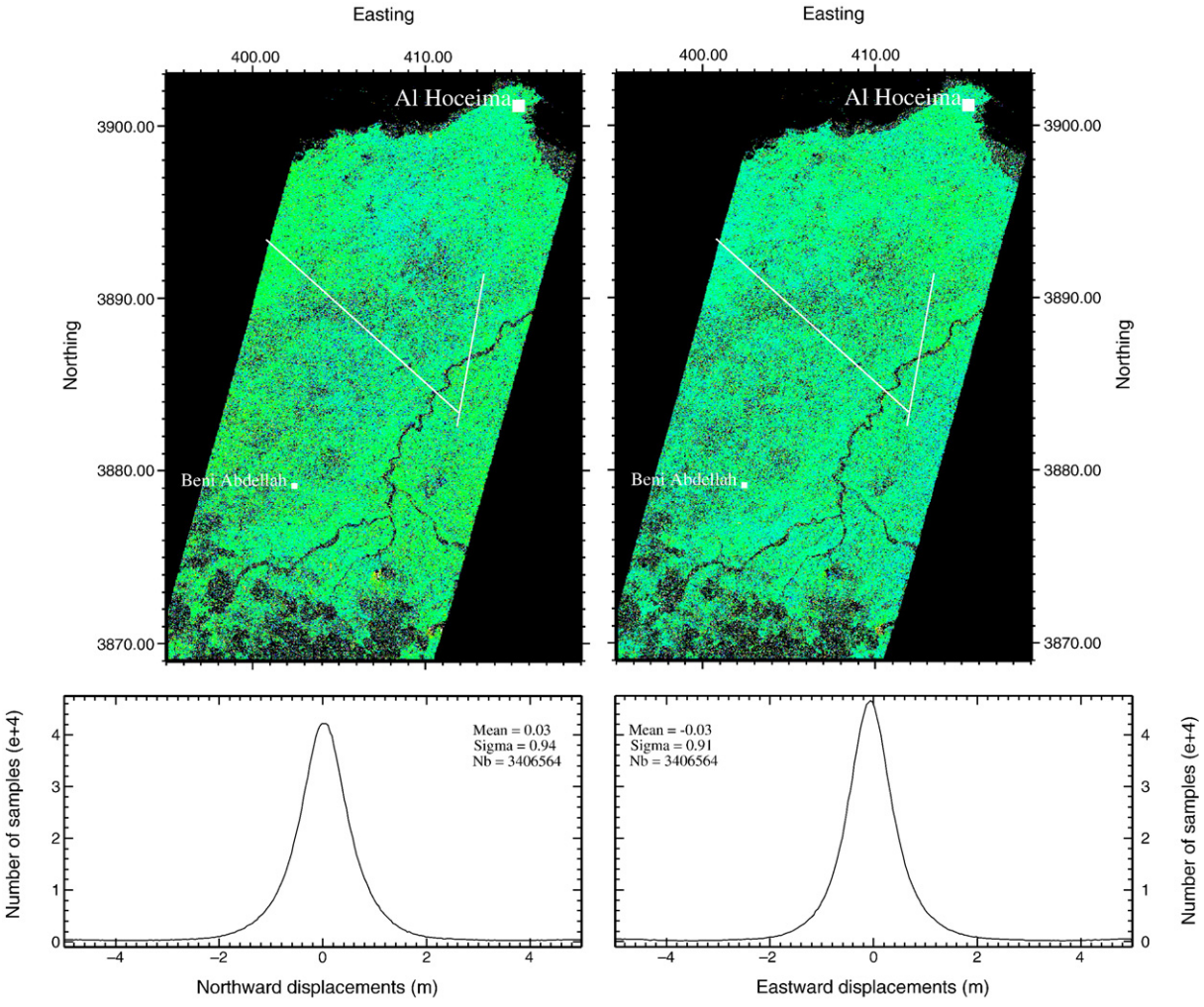

Fig. 3. SPOT5 pair images correlation results. Left: N–S component of the displacement field (up) and its corresponding histogram in the whole map (down). Right: E–W component of the displacement field (up) and its corresponding histogram in the whole map (down). The white bars are the modeled faults inferred from modelling process.

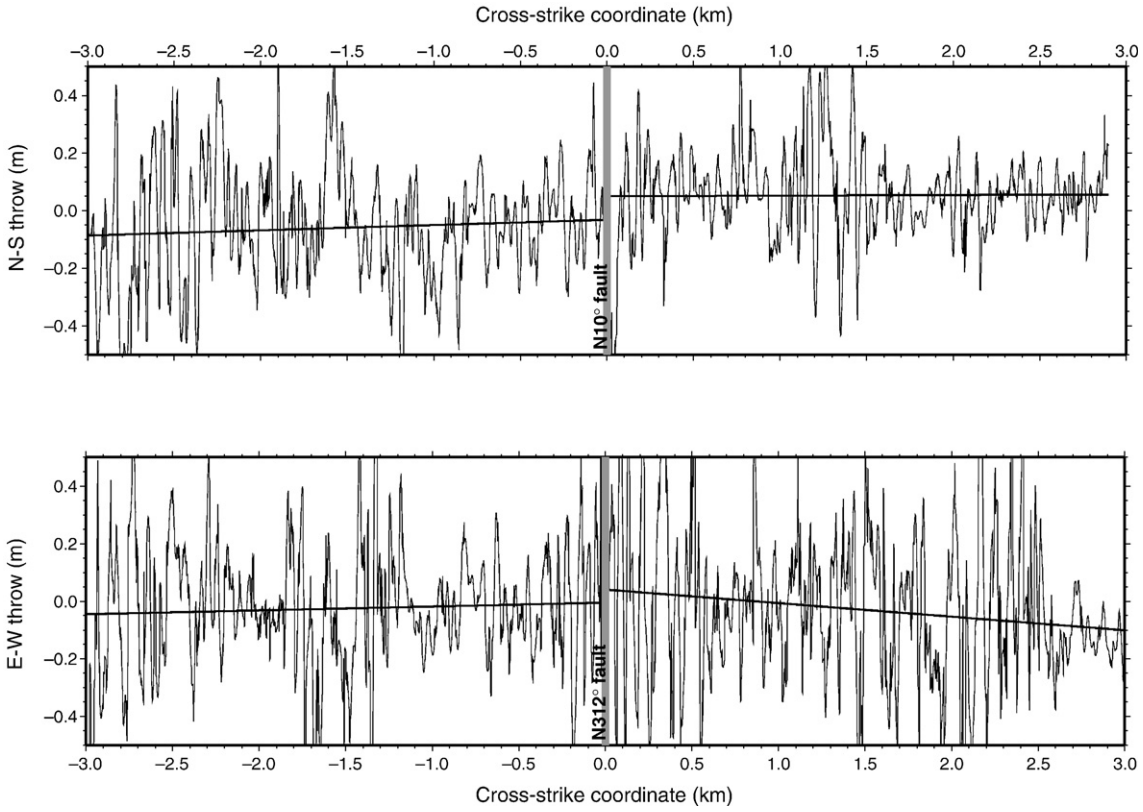

Fig. 4. (A) profile across the N10° modeled fault showing northward deformation from correlation of SPOT5 images. Straight line indicates the average trend of the profiles. The offset between the two line segments is 10±10 cm. Throw toward the North is positive. (B) profile across the N312° modeled fault showing eastward deformation. Straight line indicates the trend average of the profiles. The offset between the two line segments is 5±5 cm. Throw toward the East is positive.

likely to show a detectable offset is the E–W profile of the Northing component orthogonal to the N10° fault. Averaging the northing offset values in two distinct line segments on either side of the modeled fault striking N10°, we estimate the throw in Northing to be 5±5 cm. This value is not significantly different from zero. Indeed, similar insignificant values of throw appear in the other three profiles crossing the modeled faults, as well as in other locations. We conclude that the horizontal throw of any coseismic surface rupture can be no larger than 5 to 10 cm.

3. Slip Modeling

To explain the deformation fields estimated from the ENVISAT and SPOT5 data, we develop a theoretical model. Specifically, we seek to determine a set of earthquake source parameters. We use the formulation of Okada (1985) based on dislocations in a homogenous elastic half-space. Using a computer program to calculate coseismic displacements at the earth's surface (Feigl & Dupré, 1999), we calculate the range change values assuming the same radar line of sight at each pixel. As in previous studies, we assume that any postseismic processes occurring after 24 February 2004 are negligible. To avoid artifacts associated with overlaps between fault segments, we use simple rectangular faults. We find the best-fitting model (Fig. 5B) by a trial-and-error procedure that maximizes the length of the sum of residual phasors representing the real and imaginary parts of the phase (Vadon & Sigmundsson, 1997). When normalized by the number of pixels, this quantity is called the mean resultant length and denoted $\overline{R}$ (Mardia, 1972). For a perfect fit, the observed value and the modeled value of the phase are equal at each pixel and the mean resultant length $\overline{R}=1$. We have tuned the nine fault parameters (easting, northing, strike, depth, dip, strike slip, dip slip, length and width) to maximize R for the phase residuals in the region shown in Fig. 5.

We begin with a single rectangular dislocation varying around NE–SW left-lateral, strike-slip or around NW–SE right-lateral, strike-slip. In both cases, the misfit is unacceptably large in one orbital direction, when the best fit (minimal residual fringes) is found in the other, while also attempting to account for the GPS coseismic displacements. Both solutions require a fault with a short length (<12 km) and a large amount of strike slip (>2 m) exceeding the empirical slip-to-length ratio which is estimated to range between 0.2 to 1.0×10^{-4} for intraplate earthquakes (Scholz, 2002). The same experiment supported by an error analysis leads Biggs et al. (2006) to prefer, for simplicity, the NW–SE right-lateral plane as the primary buried fault for the 2004 Al Hoceima earthquake. In contrast, Çakir et al. (2006) prefer a curved right-lateral NW–SE striking fault. However, Stich et al. (2005) infer two subevents in the apparent source time function from waveform modelling of seismograms on two separate parallel faults striking N11° with moment magnitudes of M_w=6.2 and 6.0 for the first and second subevents, respectively. Furthermore, the aftershock distribution suggests the activation of a separate, second conjugate fault.

From these tests, we have selected a model with 18 free parameters to describe two faults that provides an acceptable fit to the InSAR, GPS, and seismic observations (Fig. 5). The first fault in the model strikes N10° with a top at a depth of 500 m and the second fault strikes N312° with a top at a depth of 3 km (Fig. 6). Their dimensions are 9×11.5 km^2 and 15×9 km^2, respectively. The slip is predominantly horizontal strike slip for both faults, with 90 cm on the N10°-striking fault and 85 cm on the N312°-striking fault (Table 1). These values of the model parameters lead to the modeled fringe patterns shown in Fig. 5B. The modeled interferograms (Fig. 5B) resemble the observed interferograms(Fig. 5A). Indeed, the residual interferograms (Fig. 5C), calculated by subtracting the modeled phase values from the observed phase values, show only a few fringes. The small number of fringes in the residual interferogram indicates that the model fits the data.

To compare our fault model with those inferred from previous studies, we calculate the residual difference between the observed phase and the modeled phase. We perform this calculation for each of

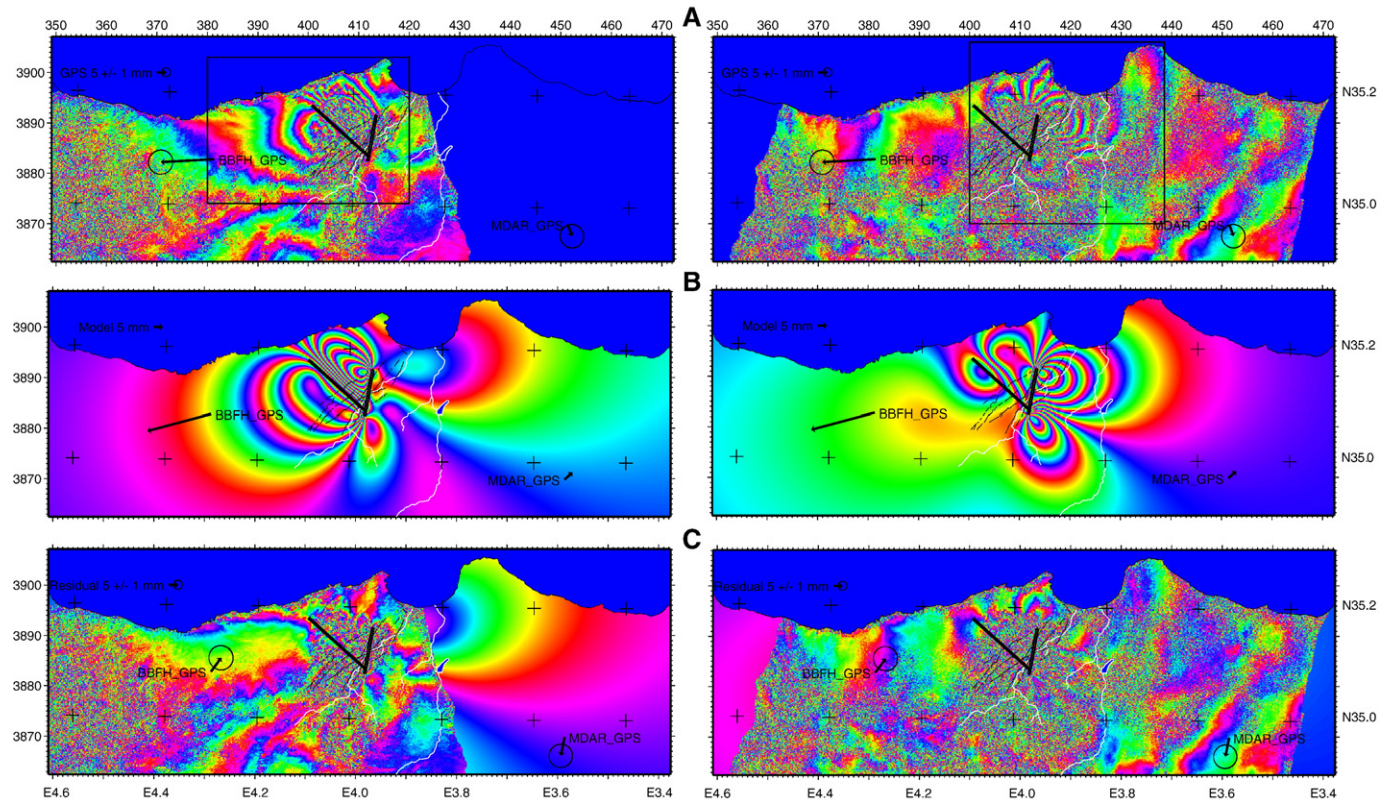

Fig. 5. Interferograms. (A) Observed InSAR interferogram from ENVISAT data, acquired in ascending (on left) and descending (on right) passes. One cycle of color represents one interferometric fringe or a range change of 28 mm along the line of sight. The black arrows indicate the coseismic horizontal displacement vectors associated with the Al Hoceima earthquake, as measured by GPS with 95% confidence ellipses. The black lines show the fissure array mapped by Aït Brahim et al. (2004). (B) Simulated fringe pattern calculated from dislocations in an elastic half-space. The black arrows indicate vectors representing the coseismic displacement at the two GPS stations calculated from the same model. (C) Residual phase calculated by substracting the modeled interferograms (B) from the observed ones (A). Vectors show the residual coseismic displacement. The two abutting two faults are plotted as black bars. The two sets of fault parameters are presented in Table 1. Rectangles in (A) delimit the near-field area used in test statistics of mean resultant length given in Table 1.

the three InSAR-based models, our two-fault model (A), the one-fault model of Biggs et al. (2006) (B), and the 25-patch model of Çakir et al. (2006) (C), as listed in Table 1, for both the ascending and descending interferograms in a small region near the epicenter where the coseismic fringes are clear (Fig. 5C).

The wrapped phase residuals vary between −1/2 and +1/2 cycles and are distributed as Von Mises (Mardia, 1972; Mardia & Jupp, 2000; Huber et al., 2001; Feigl & Thurber, 2007). A Von Mises distribution is characterized by a mean direction and a concentration parameter κ. We perform a two-sample test to test the null hypothesis that the concentration parameters of two sets of residuals are equal, assuming that their mean directions are both null (Mardia & Jupp, 2000). This test involves calculating the mean resultant length $\overline{R}$ for each set of residuals, as shown in the final column of Table 1. These values account for a total of 293644 pixels in the near-field parts of the ascending and descending interferograms.

Since $\overline{R}$ <0.45 in all cases, we use the statistic given by equation (7.3.23) of Mardia & Jupp (2000). It is normally distributed with zero mean and unit variance. First, we test the null hypothesis H_0 that the concentration parameter for the residuals equals the concentration parameter for the observations. The test statistic takes the values −10.1, −1.1, and +10.8 for the residuals for models A, B, and C, respectively. Accordingly, we reject the null hypotheses $H_0\{\kappa(A)=\kappa(Z)\}$ and $H_0\{\kappa(C)=\kappa(Z)\}$ with 95% confidence. In other words, our 2-fault model fits the data better than does the zero Z model; the 1-fault model of Biggs et al. (2006) does not fit the data; and the 25-patch model of Çakir et al. (2006) fits the data worse than the zero model.

Next we compare the residuals from models B and C to those from A. The test statistics for null hypothesis $H_0\{\kappa(B)=\kappa(A)\}$ and $H_0\{\kappa(C)=\kappa(A)\}$ are +12.2 and +6.7 respectively, rejecting both of them. Accordingly, we conclude that the two-fault A model fits the data significantly better than either model B of Biggs et al. (2006) or model C of Çakir et al. (2006), with 95% confidence.

4. Ground truth observations

4.1. GPS surveys

GPS data from two stations established prior to the 24 February 2004 earthquake near the epicentral zone, have been used to measure the coseismic displacements. Both are part of the Moroccan GPS network, where measurements have been performed since 1999. To study the coseismic motion that occurred during the 2004 Al Hoceima earthquake, one must first account for the long-term secular motion that occurred prior to it. The NUVEL-1A model and GPS velocity measurements predict convergence between the Africa and Eurasia plates in this region at a rate of 3 to 5 mm/yr directed roughly NW–SE (DeMets et al., 1994; Calais et al., 2003; McClusky et al., 2003).

Recent results from the Moroccan GPS network suggest three distinct blocks in the Rif domain (Fadil et al., 2006; Tahayt et al., 2008). These blocks are, from West to East, the Tangier block, the Central Rif block and the Oriental Rif block. The Al Hoceima seismic zone is situated between the Central Rif and the Oriental Rif, accommodating 3.4±1.2 mm/yr of motions due to the Africa-Eurasia plate convergence. Two stations near Al Hoceima, BBFH and MDAR, show velocities of 3.3±2.0 mm/yr toward the SW and 2.3±2.0 mm/yr toward the NE with respect to Africa, respectively during the time interval leading up to the earthquake (Fig. 1). The GPS station at BBFH

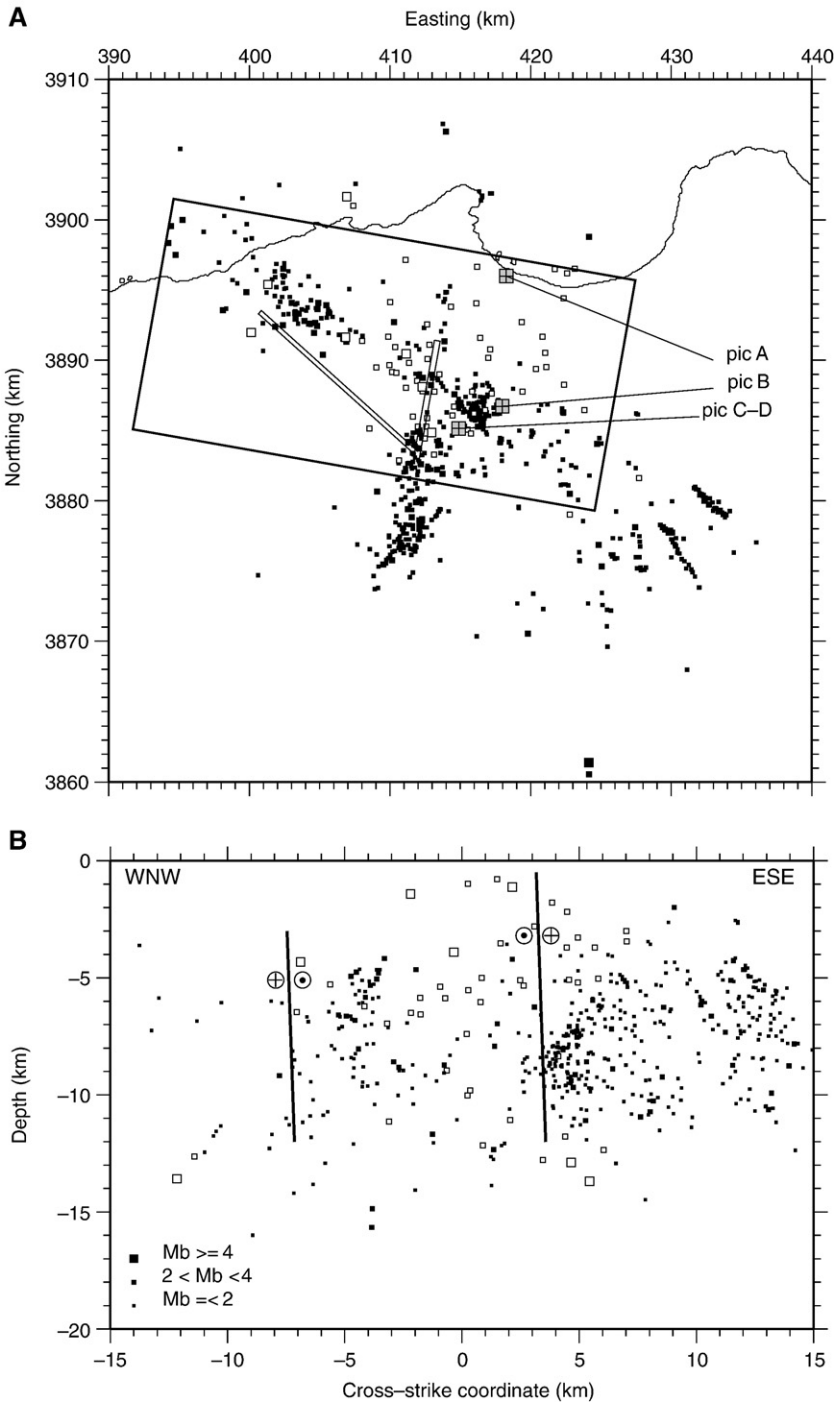

Fig. 6. (A) Location of recorded aftershocks during the two week period following the 24 February 2004 Al Hoceima earthquake. Bars are the two modeled faults. Rectangle indicates the cross-section frame. picA, picB and picC-D indicate location of photographs presented in Fig. 7A–C and 7D, respectively. (B) Cross-section oriented WNW–ESE and centred on the epicentral area, showing the distribution of aftershocks at depth around the two modeled faults. To the left is the N312° fault with predominantly right-lateral strike-slip, the top of which is located 3 km below the surface. To the right is the N10° fault with predominantly left-lateral strike-slip, the top of which is located 500 m below the surface. In both panels, filled black symbols denote relocated aftershocks recorded by the temporary array installed after the mainshock. The open symbols denote early aftershocks located using only data from the permanent seismologic stations.

is located 30 km to the west of the Al Hoceima seismic zone on the Central Rif block. The MDAR station sits 40 km to the southeast of the Al Hoceima seismic zone on the Oriental Rif block.

The two GPS stations were measured before the 24 February 2004 earthquake in February 2001, October 2001, and October 2002, each time for 24-hour sessions. After the earthquake in 2004, the two stations were measured from 26 February, for five days and then again in October 2004 for 24 h. The GPS data were analyzed with the GAMIT/GLOBK software package (Herring, 2002; King & Bock, 2004) to obtain the coseismic displacement vectors at BBFH and MDAR on the day of the mainshock. The station positions were extrapolated to the time of the mainshock, before differencing, to calculate the coseismic displacement, as described in Reilinger et al. (2000) for the Izmit earthquake. While BBFH experienced a horizontal displacement of 30±4 mm toward the west, MDAR has an insignificant displacement of 5±4 mm (Fig. 5).

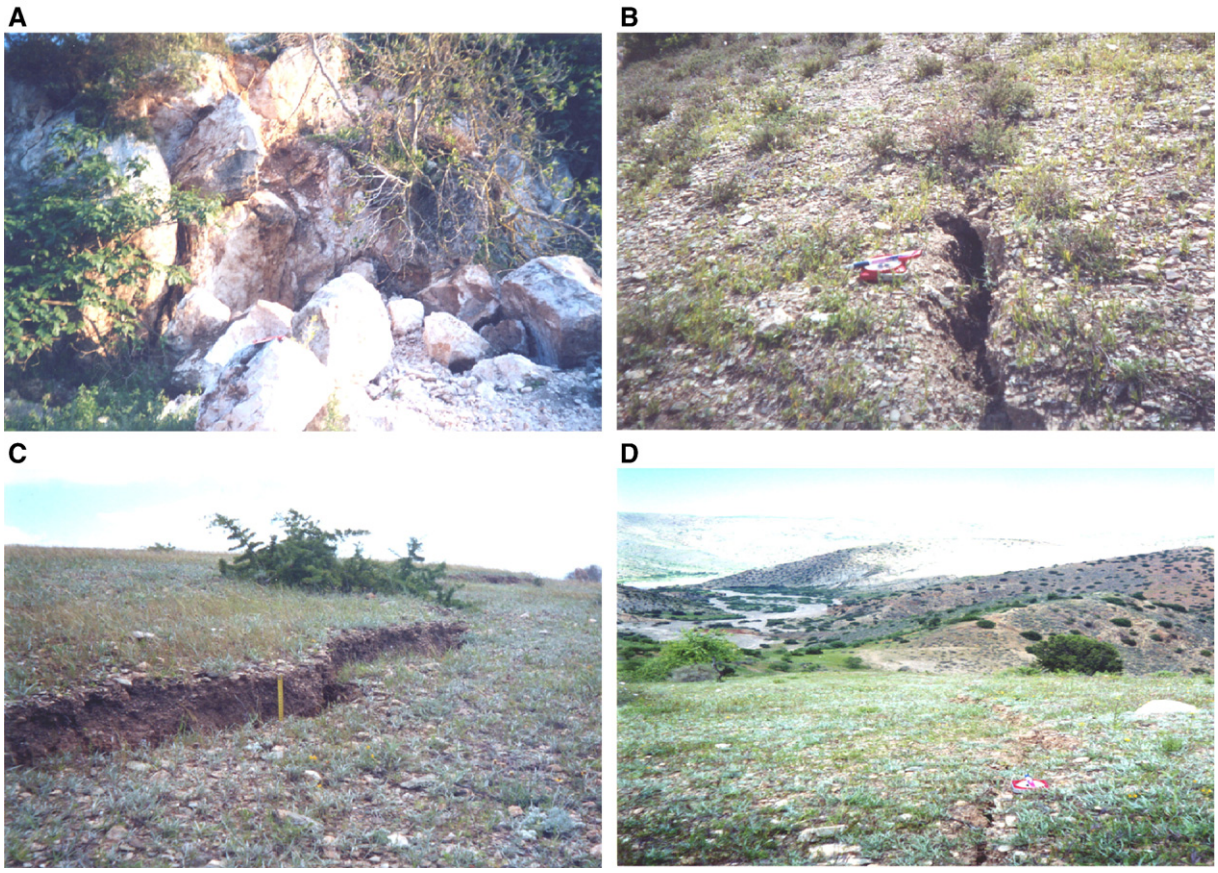

Fig. 7. Photos in the damaged area around Al Hoceima taken in March 2004. (A) rock falls near Club Med 8 km south-east of Al Hoceima city, (B) tension crack (12 cm wide) looking WSW in Iffassyen village 20 km south of Al Hoceima city, (C) secondary rupture looking south observed in Amrabten region 22 km south of Al Hoceima. The western side dropped, (D) the same surface rupture looking north. The throw is 25 cm, west side dropped. See locations in Fig. 6A.

4.2. Previous seismological studies

Previous seismological determinations of the source parameters for the 2004 Al Hoceima main shock indicate predominately strike-slip rupture (Fig. 2). To investigate the source, Stich et al. (2005) used a set of Apparent Source Time Functions (ASTFs) with total duration of 5 to 6 s and concluded that the 2004 Al Hoceima main shock consisted of two consecutive subevents separated by about 3 s. They find similar focal mechanisms and parallel faults for the two subevents, although the relative locations are poorly constrained. The source time function estimated by Biggs et al. (2006) suggests a longer rupture history that can be separated into several discrete pulses.

4.3. Aftershock locations

Twenty autonomous seismological stations were deployed during two weeks following the main shock in the epicentral zone of Al Hoceima. The network is shown in Fig. 2. Aftershock magnitudes were determined from the coda length using the common relation $M_d = 2\ \mathrm{Log}\ \tau - 0.87$, where τ is the coda length in seconds. This array allows us to locate most of the 650 aftershock events of magnitude ranging from 0.5 to 4. In addition, we relocated the early aftershocks that occurred before installing the temporary array with $M_b > 3.5$ using data from the Moroccan (CNRST, 2004) and Spanish (IGN, 2004) stations. The relocated aftershocks define a complex geometry with two principal directions, trending NNE–SSW and NW–SE, that are roughly perpendicular (Fig. 6A). These directions are compatible with both fault planes in the focal mechanism provided by the USGS. The aftershocks are distributed differently at depth around the two possible nodal planes. The NNE–SSW plane appears to have ruptured during the main shock, in agreement with macroseismic observations (Dorbath et al., 2005). None of the relocated aftershock hypocenters is shallower than 2 km in depth (Fig. 6B). Focal mechanisms for 70 of the aftershocks have been estimated. They show a horizontal minimal stress axis oriented N70° as well as maximal stress that is horizontal and orthogonal, reflecting the strike-slip tectonic regime (Dorbath et al., 2005).

4.4. Geological observation of surface ruptures in the field

On April 2004, we investigated the free surface damaged zone, searching for any evidence of the fault rupture associated with the main shock. No clear primary seismically ruptured surface has been observed. The fissures mapped by Aït Brahim et al. (2004) define a zone starting at Al Hoceima Bay and continuing about 25 km to the SSW–SW. Minor cracks of orthogonal directions (NNW–SSE to NW–SE) have also been observed in the epicentral area (Fig. 6A).

Most of the observed features are tensile cracks that opened between 2 and 10 cm. In addition to landslides and rock falls triggered by the earthquake, several breaks of a hundred meters in length show small scarps with throws as large as 25 cm in some places. Fig. 7 shows some of these surface effects.

5. Discussion

To fit the INSAR data, we suggest a model with two abutting, conjugate faults (Fig. 8). INSAR provides a strong constraint on the location and geometry of the faults. The location and parallel geometry of the two faults suggested by Stich et al. (2005) arenot compatible with the deformation pattern observed in the coseismic interferograms. While the strike of N11° is close to one fault (N10°) in our model, the strike of the second event in our model is perpendicular to theirs. However, because seismic observations from

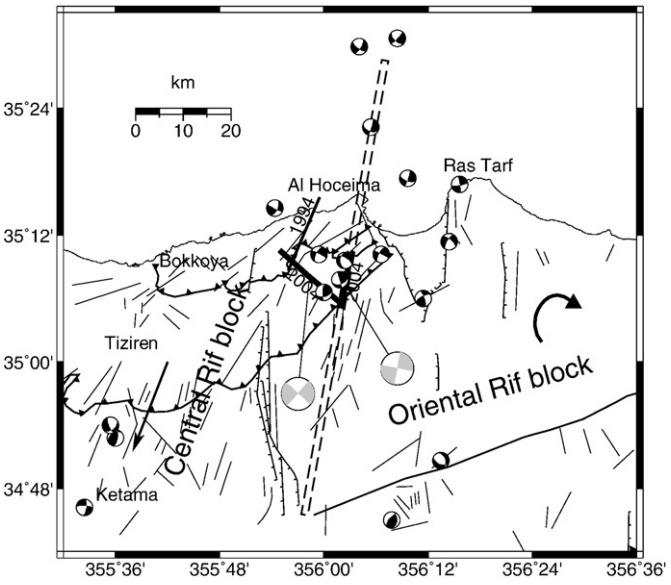

Fig. 8. Tectonic interpretation of the cross-fault model (thick bars) inferred in this study. Their corresponding focal mechanisms are represented by gray beachballs. Dashed line is our interpretative trend of the cross-fault system separating the Central Rif block from the Oriental Rif block distinguished recently from GPS analysis (Fadil et al., 2006; Tahayt et al., 2007). Arrows indicate the relative movements of these blocks with respect to the Africa plate. The 1994 rupture is from Akoglu et al. (2006). Other tectonic features as in Fig. 1.

stations distributed mostly on the north side of the epicenter, as used by Stich et al. (2005), cannot distinguish between conjugate fault planes, our two-fault model is compatible with both the geodetic and seismological observations.

The correlation of SPOT5 images, with dm-level of uncertainty as used here, confirms that the Al Hoceima rupture did not reach the free surface. From previous work, we estimate that this technique could detect a coherent surface throw as small as 0.2 pixel or 50 cm with the SPOT5 images used here. For example, throws of 3 m during the Izmit earthquake (1999), 0.8 m during the Bam earthquake (2003) and 5 m during the Kashmir earthquake were all clearly detected by correlating, respectively, 10-m resolution SPOT images (Feigl et al., 2002), 2.5-m resolution SPOT5 images (Binet & Bollinger, 2005) and 15-m resolution ASTER images (Avouac et al., 2006). In the case of Al Hoceima, the correlation of the two SPOT5 images confirms that no surface rupture with a throw larger than 50 cm occurred during the Al Hoceima earthquake. By averaging the offset values in profiles across the modeled faults, we can tighten this bound to 5–10 cm (Fig. 4). Indeed, in its limit of applicability, optical image correlation allows us to exclude any principal surface rupture. In other words, if the 85 cm of slip we infer from the InSAR data reached the surface, it would appear as a significant offset in the SPOT correlation results presented in Figs. 3 and 4.

A similar "cross-fault" model has been suggested by Hudnut et al. (1989) in the Superstition Hills, southern California, to explain the occurrence of two M_w>6 events there in 1987. There, the two earthquakes occurred on distinct faults with surface offsets. Their epicenters were 10 km apart. In the case of Al Hoceima, such a cross-fault model appears to be compatible with the seismologic and geodetic data considered here.

On the other hand, the strikes of the two candidate fault planes are difficult to reconcile with the orientation of the surface ruptures observed in the field. One possibility is that the small fissures and scarps are secondary features caused by slumping and downhill motion of soil and unconsolidated sediments during the earthquake shaking. Another, more speculative, possibility is that the free surface changes the orientation of the stress field such that the fissures at the surface form an acute angle with the fault plane. Although angles of 10° to 20° have been observed and can be explained by Riedel shear (Scholz, 2002), the angle at Al Hoceima is at least 35° to 40°. Such large angles can develop in some theoretical models (Belardinelli et al., 2000; Dalguer et al., 2003). The angle between the surface fracture arrays and the main fault is roughly proportional to the coefficient of friction, and therefore depends on local conditions, including pore fluid pressure, near the free surface.

Abutting faults have also been inferred in other earthquakes. For the Bam (Iran) 2003 earthquake, two subevents ruptured two parallel right-lateral strike-slip faults intersecting at depth based on InSAR observations (Funning et al., 2005). Two subevents were also inferred from broadband body wave seismograms (Jackson et al., 2006). Yet Stramondo et al. (2005) propose a single rectangular fault plane. From this example, it is clear that extra information from other techniques can be helpful to constrain model parameters along with the InSAR data.

Regarding the timing of the rupture within the Al Hoceima pair of faults on February 2004, Stich et al. (2005) suggest that the rupture events on the two parallel N11° faults in their model are separated by 3 s. In our model, we suggest that the rupture initiated in the N10° plane and then transferred to the N312°-striking fault. Although the geodetic measurements cannot constrain this time delay, it seems likely that the stress concentration on both planes triggered the aftershocks (Fig. 6). We find geodetic moments of 2.80×10^{18} N m for the N10° plane, and 3.08×10^{18} N m for the N312° plane. Consequently, the geodetic moment magnitude is M_w=6.3 for each of the two events, assuming a shear modulus of 30 GPa. These values are slightly larger than those (M_w=6.2 and M_w=6.0) estimated from waveform inversion by Stich et al. (2005). The geodetic estimate of moment is larger than the seismological estimate, as observed in other earthquakes (Feigl, 2002).

The NW–SE cluster of aftershocks does not appear to align with the N312° striking fault (Fig. 6). This result does not contradict our model. Most of the locations of the events in the SE part of this area have large uncertainties because they occurred before the temporary array of seismometers was installed. These early events were located using only seismograms recorded in the first few days following the mainshock at permanent stations. The later events recorded by our dense network have smaller uncertainties in location than the early events (Fig. 2 and 6). The apparent discrepancy posed by this cluster may also be due to complexities in local geology and seismic velocity.

Such a complex rupture with two subevents has occurred before in the Al Hoceima region. Bezzeghoud & Buforn (1999) distinguished two subevents for the 1994 earthquake from body wave inversion and suggested two faults striking N–S and NNW–SSE. Recently, both Biggs et al. (2006) and Akoglu et al. (2006) have suggested a cross-fault model for this area by combining the 1994 and 2004 faults. Biggs et al. (2006) also discuss the geometric similarity between the 1987 Superstition Hills earthquake pair (Hudnut et al., 1989) and the 1994–2004 Al Hoceima pair. They point out that the stress transfer needed in a cross-fault mechanism can take a long time. In the first case, the time delay was 11 h; in the latter case it was 10 years. During the 2004 Al Hoceima mainshock, the delay was only 3 s between the two subevents (Stich et al., 2005).

6. Conclusions

INSAR data from the ENVISAT satellite have been used to constrain a model for the source mechanism of the Al Hoceima earthquake in 2004. Simple fault models with only a single slip patch do not fit the interferograms well. Tests with two faults indicate that rupture was related to a cross-fault mechanism, supported by the two subevents inferred from seismology. We suggest that the rupture initiated on the N10° left-lateral strike-slip fault and transferred to the N312° right-lateral strike-slip fault. The moment magnitude inferred from our model is M_w=6.3 for each of the two subevents. Comparison with previous studies indicates that the two-fault model inferred here fits the InSAR data better than two other published models. Neither of the

hypothesized faults of the 2004 Al Hoceima earthquake appear to have ruptured the surface. This interpretation is supported by the optical remote sensing data from SPOT5, as well as with ground based observations by geodesy, seismology and geology.

We suggest that the pair of crossed faults activated in 2004 is part of a complex buried faults system trending roughly NNE–SSW. As sketched in Fig. 8 and discussed above (Sections 1 and 4.1), this fault system plays an important role in accommodating the relative block motions within the present-day tectonic regime (Fadil et al., 2006; Tahayt et al., 2008). A more detailed study of stress changes in this region is needed to evaluate the seismic hazard in this populated area.

Acknowledgments

We gratefully acknowledge the generous assistance during difficult times following the earthquake of all the people who helped us to carry out the field campaigns. We thank Jose Martin Davila and Jorge Garrate (Real Instituto y Observatorio de la Armada, Cadix, Spain) for sharing GPS data. We thank Ziyadin Çakir (Istanbul Technical University, Istanbul, Turkey) for generously providing his model parameters for comparison. We also thank Jean-Philippe Avouac and three other reviewers for constructive criticism. The ENVISAT data were provided by the European Space Agency under a Category-I project to F. Gomez. The SPOT5-HRG images purchased under a price reduction granted by the ISIS program (ISIS0403-620). This study was supported in part by a bilateralFranco-Moroccan Thesis Fellowship from the Agence Universitaire de la Francophonie to A. Tahayt and NSF Grant EAR-0408728 to MIT (R.R. and S.M.). All figures in this paper were made with the Generic Mapping Tools (Sandwell & Smith, 1991).

References

Aït Brahim, L., Nakhcha, C., Tadili, B., El Mrabet, T., & Jabour, N. (2004). Structural analysis and interpretation of the surface deformations of the February 24th 2004 Al Hoceima earthquake. *European-Mediterranean Seismic Centre Newsletter*, *21*, 10–12.

Akoglu, A. M., Çakir, Z., Meghraoui, M., Belabbes, S., El Alami, S. O., Ergintav, S., et al. (2006). The 1994–2004 Al Hoceima (Morocco) earthquake sequence: conjugate fault ruptures deduced from InSAR. *Earth and Planetary Sciences Letters*, *252*, 467–480.

Avouac, J. P., Ayoub, F., Leprince, S., Konca, O., & Helmberger, D. V. (2006). The 2005, M_w 7.6 Kashmir earthquake: sub-pixel correlation of ASTER images and seismic waveforms analysis. *Earth and Planetary Sciences Letters*, *249*, 514–528.

Belardinelli, M. E., Bonafede, M., & Gudmunsson, A. (2000). Secondary earthquake fractures generated by a strike slip fault in the South Iceland Seismic Zone. *Journal of Geophysical Research*, *105, B6*, 13613–13629.

Berthier, E., Vadon, H., Baratoux, D., Arnaud, Y., Vincent, C., Feigl, K. L., et al. (2005). Surface motion of mountain glaciers derived from satellite optical imagery. *Remote Sensing of Environment*, *95*(1), 14–28.

Bezzeghoud, M., & Buforn, E. (1999). Source parameters of the 1992 Melilla (Spain, M_w = 4.8), 1994 Al Hoceima (Morocco, M_w = 5.8) and Mascara (Algeria, M_w = 5.7) earthquakes and seismotectonic implications. *Bulletin of Seismological Society of America*, *89*, 359–372.

Biggs, J., Bergman, E., Emmerson, B., Funning, J. G., Jackson, J., Parsons, B., et al. (2006). Fault identification for buried strike-slip earthquakes using InSAR: the 1994 and 2004 Al Hoceima. *Morocco earthquakes, Geophysical Journal International*, *166*, 1347–1362.

Binet, R., & Bollinger, L. (2005). Horizontal coseismic deformation of the 2003 Bam (Iran) earthquake measured from SPOT5 THR satellite imagery. *Geophysical Research Letters*, *249*(3–4), 514–528.

Çakir, Z., Meghraoui, M., Akoglu, A. M., Jabour, N., Belabbes, S., & Aït Brahim, L. (2006). Surface deformation associated with the M_w 6.4, 24 February 2004 Al Hoceima, Morocco, earthquake deduced from InSAR: implications for the active tectonics along North Africa. *Bulletin of Seismological Society of America*, *96*(1), 59–68.

Calais, E., DeMets, C., & Nocquet, J. M. (2003). Evidence for a post-3.16- Ma change in Nubia Eurasia-North America plate motions? *Earth and Planetary Sciences Letters*, *216*, 81–92.

Calvert, A., Gomez, F., Seber, D., Barazangi, M., Jabour, N., Ibenbrahim, A., et al. (1997). An integrated geophysical investigation of recent seismicity in the Al Hoceima Region of North Morocco. *Bulletin of Seismological Society of America*, *87*, 637–651.

CNRST (2004). *Centre National pour la Recherche Scientifique et Technique, Moroccan seismic network.* http://sismo-lag.cnrst.ma/

Dalguer, L. A., Irikura, K., & Riera, J. D. (2003). Simulation of tensile crack generation by three-dimensional dynamic shear rupture propagation during an earthquake. *Journal of Geophysical Research*, *108*(B32144). doi:10.1029/2001JB001738.

Delacourt, C., Allemand, P., Berthier, E., Raucoules, D., Casson, B., Grandjean, P., et al. (2007). Remote sensing techniques for analyzing landslide kinematics: a review. *Bulletin de la Societé Géologique de France*, *178*(2), 89–100.

DeMets, C., Gordon, R., Argus, D., & Stein, S. (1994). Effect of recent revisions to the geomagnetic reversal time scale on estimates of current plate motions. *Geophysical Research Letters*, *21*, 2191–2194.

Dorbath, L., Hahou, Y., Delouis, B., Dorbath, C., Van Der Woerd, J., Bardrane, S., et al. (2005). Etudes sismologiques sur le séisme D'Al Hoceima: localisation, et mécanisme du choc principal et des répliques, contraintes et structure de la zone epicentrale. Communication, Colloque Intenational "Séisme d'Al Hoceima: bilan et perspectives", 24–26 February 2005, Al Hoceima, Morocco.

El Alami, S. O., Tadili, B., Cherkaoui, T. E., Medina, F., Ramdani, M., Aït Brahim, L., et al. (1998). The Al Hoceima earthquake of May. *26, 1994 and its aftershocks: a seismotectonic study, Annali di Geofisica*, *41*, 519–537.

El Mrabet, T. (2005). The great earthquakes in the Maghreb region and their consequences on man and environment (in Arabic with abstract in English). *Edit. Centre National de Recherche Scientifique et Technique, Rabat, Morocco.*

Fadil, A., Vernant, P., McClusky, S., Reilinger, R., Gomez, F., Ben Sari, D., et al. (2006). Active tectonics of the western Mediterranean: geodetic evidence for roll back of a delaminated subcontinental lithospheric slab beneath the Rif mountains (Morocco). *Geology*, *34*(7), 529–532.

Falorni, G., Teles, V., Vivoni, E. R., Bras, R. L., & Amaratunga, K. S. (2005). Analysis and characterization of the vertical accuracy of digital elevation models from the shuttle radar topography mission. *Journal of Geophysical Research*, *110*(F02005). doi:10.1029/2003JF000113.

Feigl, K.L. & Thurber, C.H., (2007). A technique for modeling radar interferograms without phase unwrapping: Application to the M 5 Fawnskin, California earthquake of 4 December 1992, *Geophysical Journal International*, in press.

Feigl, K. L. (2002). Measurement of coseismic deformation by satellite geodesy. In W. H. K. Lee, H. Kanamoori, & P. C. Jennings (Eds.), *International Handbook of Earthquake and Engineering Seismology*, *81A* (pp. 607-620). Academic Press.

Feigl, K. L., Sarti, F., Vadon, H., McClusky, S., Ergintav, S., Durand, P. h., et al. (2002). Estimating slip distribution for the izmit mainshock from coseismic GPS, ERS-1, RADARSAT, and SPOT measurements. *Bulletin of Seismological Society of America*, *92*(1), 138–160.

Feigl, K. L., & Dupré, E. (1999). RNGCHN: a program to calculate displacement components from dislocations in an elastic half-space with applications for modeling geodetic measurements of crustal deformation. *Computers & Geosciences*, *25*, 695–704.

Frizon de Lamotte, D., Andrieux, J., & Guezou, J. C. (1991). Cinematique des chevauchements neogènes dans l'Arc bético-rifain; discussion sur les modèles geodynamiques. *Bulletin de la Societé Géologique de France*, *162*, 611–626.

Funning, G. J., Parsons, B., Wright, T. J., Jackson, J. A., & Fielding, E. J. (2005). Surface displacements and source parameters of the 2003 Bam (Iran) earthquake from Envisat advanced synthetic aperture radar imagery. *Journal of Geophysical Research*, *110*(B09406). doi:10.1029/2004JB003338.

Hahou, Y. (2005). Sismicité du Maroc, apport de l'étude des séismes d'Al Hoceima et de Rissani et évaluation de l'aléa sismique, Ph.D. Thesis, Université Mohamed V, Rabat, Morocco.

Harvard CMT (2005). *Centroid Moment Tensor Project, On-line Catalog.* http://www.globalcmt.org/CMTsearch.html

Hatzfeld, D., Caillot, V., Cherkaoui, T. E., Jebli, H., & Medina, F. (1993). Microearthquake seismicity and fault plane solutions around the Nekor strike-slip fault, Morocco. *Earth and Planetary Sciences Letters*, *120*, 31–34.

Herring, T. A. (2002). *GLOBK: Global Kalman filter VLBI and GPS analysis program, Version 10.0.* Cambridge: Massachussetts Institute of Technology.

Huber, R., Dutra, L. V., & da Costa Freitas, C. (2001). SAR interferogram phase filtering based on the Von Mises distribution. *Geoscience and Remote Sensing Symposium, 2001. IGARSS '01. IEEE 2001 International*, *vol. 6*. (pp. 2816–2818).

Hudnut, K. W., Seeber, L., & Pacheco, J. (1989). Cross-fault triggering in the November 1987 Superstition Hills earthquake sequence, southern California. *Geophysical Research Letters*, *16*, 199–202.

IGN (2004). *Instituto Geográfico Nacional, Spanish seismic network.* http://www.ign.es/ign/en/IGN/home.jsp

Jabour, N., Kasmi, M., Menzhi, M., Birouk, A., Hni, L., Hahou, Y., et al. (2004). The February 24th, 2004 Al Hoceima earthquake. *European-Mediterranean Seismic Centre Newsletter*, *21*, 7–10.

Jackson, J., Bouchon, M., Fielding, E., Funning, G., Ghorashi, M., Hatzfeld, D., et al. (2006). Seismotectonic, rupture process, and earthquake-hazard aspects of the 2003 December 26 Bam, Iran, earthquake. *Geophysical Journal International*, *166*, 1270–1292.

King, R. W., & Bock, Y. (2004). *Documentation for GAMIT analysis software, release 10.2.* Cambridge: Massachusetts Institute of Technology.

Leblanc, D., & Olivier, P. h. (1984). Role of strike-slip faults in the Betic-Rifian orogeny. *Tectonophysics*, *101*, 345–355.

Leprince, S., Barbot, S., Ayoub, F., & Avouac, J. P. (2007). Automatic and precise orthorectification, coregistration, and subpixel correlation of satellite images, application to ground deformation measurements. *IEEE Transactions on Geoscience and Remote Sensing*, *45*(6), 1529–1557.

Mardia, K. V. (1972). *Statistics of Directional Data.* London: Academic Press 375 pp.

Mardia, K. V., & Jupp, P. E. (2000). *Directional statistics.* New York: J. Wiley & Sons 429 pp.

Massonnet, D., Rossi, M., Carmona, C., Adragna, F., Peltzer, G., Feigl, K., et al. (1993). The displacement field of the Landers earthquake mapped by radar interferometry. *Nature*, *364*, 138–142.

Massonnet, D., & Rabaute, T. (1993). Radar interferometry: limits and potential. *IEEE Trans. Geoscience & Remote Sensing*, *31*, 455–464.

Massonnet, D., & Feigl, K. L. (1998). Radar interferometry and its application to changes in Earth's surface. *Reviews of Geophysics*, *36*(4), 441–500.

McClusky, S., Reilinger, R., Mahmoud, S., Ben Sari, D., & Tealeb, A. (2003). GPS constraints on Africa (Nubia) and Arabia plate motions. *Geophysical Journal International*, *155*, 126–138.

Michel, R., & Avouac, J. P. (2002). Deformation due to the 17 August 1999 Izmit, Turkey, earthquake measured from SPOT images. *Journal of Geophysical Research*, *107*(B4), 2062. doi:10.1029/2000JB000102.

NASA/SRTM (2005). *SRTM3: Shuttle Radar Topography Mission digital topographic data.* Version2, ftp://e0srp01u.ecs.nasa.gov/srtm/version2/SRTM3/

Okada, Y. (1985). Surface deformation to shear and tensile faults in a half-space. *Bulletin of Seismological Society of America*, *75*(4), 1135–1154.

Reilinger, R. E., Ergintav, S., Bürgmann, R., McClusky, S., Lenk, O., Barka, A., et al. (2000). Coseismic and postseismic fault slip for the 17 August 1999. *M = 7.5, Izmit, Turkey earthquake, Science*, *289*, 1519–1524.

Sandwell, D. T., & Smith, W. H. (1991). Free software helps map and display data, EOS Transactions.*Amererican Geophysical Union*, *72*(41), 445–446, http://gmt.soest.hawaii.edu/

Scharroo, R., & Visser, P. (1998). Precise orbit determination and gravity field improvement for the ERS satellites. *Journal of Geophysical Research*, *103*(C4), 8113–8127.

Scholz, C. H. (2002). *The Mechanics of Earthquakes and Faulting*, 2nd ed. Cambridge, U.K.: Cambridge University Press.

Service Géologique du Maroc, Rabat (1992). Carte des mouvements récents du Rif. *Notes et Mémoires*, 365.

Stich, D., Mancilla, F., Baumont, D., & Morales, J. (2005). Source analysis of the M_w 6.3 2004 Al Hoceima earthquake (Morocco) using regional apparent source time functions. *Journal of Geophysical Research*, *110*(B06306). doi:10.1029/2004/B003366.

Stich, D., Ammon, C. J., & Morales, J. (2003). Moment tensor solutions for small , moderate earthquakes in the Ibero-Maghreb region. *Journal of Geophysical Research*, *108*(B3). doi:10.1029/2002JB002057.

Stramondo, S., Moro, M., Tolomei, C., Cinti, F. R., & Doumaz, F. (2005). InSAR surface displacement field and fault modelling for the 2003 Bam earthquake (southeastern Iran). *Journal of Geodynamics*, *40*, 347–353.

Tahayt, A., Mourabit, T., Rigo, A., Feigl, K. L., Fadil, A., McClusky, S., et al. (2008). Present-day movements of tectonic blocks in the Betic-Rif Arc from GPS measurements 1999–2005. *Comptes Rendus Geoscience*, *340*, 400–413. doi:10.1016/j.crte.2008.02.003.

Vadon, H., & Sigmundsson, F. (1997). Crustal deformation from 1992 to 1995 at the mid-atlatic ridge, Southwest Iceland, mapped by satellite radar interferometry. *Science*, *275*, 193–197.

Van Puymbroeck, N., Michel, R., Binet, R., Avouac, J. P., & Taboury, J. (2000). Measuring earthquakes from optical satellite images. *Applied Optics*, *39*(20), 3486–3494.